Available online at www.sciencedirect.com
SCIENCE DIRECT®
Journal of Catalysis 222 (2004) 481–492
JOURNAL OF CATALYSIS
www.elsevier.com/locate/jcat

Catalytic dehydrogenation of alkanes on Pt/Na-[Fe]ZSM5 and staged O_2 introduction for selective H_2 removal

Toshio Waku,[a,1] Joseph A. Biscardi,[b] and Enrique Iglesia [a,*]

[a] *Department of Chemical Engineering, University of California at Berkeley, Berkeley, CA 94720, USA*
[b] *ChevronTexaco Energy Research and Technology Co., Richmond, CA 94802, USA*

Received 4 August 2003; revised 18 December 2003; accepted 18 December 2003

Abstract

Small Pt clusters within Na-[Fe]ZSM5-protected channels catalyze C_3H_8 and C_2H_6 dehydrogenation with unprecedented turnover rates and catalyst stability. Alkene selectivities are greater than 97% at near-equilibrium alkane conversions. Mild oxidative treatments fully restored initial catalytic rates and selectivities. Exchange sites in Na-[Fe]ZSM5 lead to well-dispersed Pt precursors and catalytic Pt clusters, which reside within ZSM5 channels that inhibit the formation of large unreactive organic residues. The weak acidity of residual OH groups in [Fe]ZSM5 minimizes β-scission and oligomerization reactions, which lead to loss of alkene selectivity and to unreactive organic residues. Thermodynamic constraints were removed by selective combustion of H_2 using O_2 coreactants. More than 90% of the O_2 introduced was used to form H_2O from H_2, even when hydrocarbons were the predominant available reactants. Equivalent O_2 amounts cofed with C_3H_8 reactants led instead to $\sim 5\%$ selectivity for H_2 combustion. Hydrocarbon combustion was the predominant reaction and the cofed O_2 was depleted before H_2 could be formed and dehydrogenation approached equilibrium. Alkene yield enhancements of ~ 1.6 above equilibrium were achieved by selective H_2 removal using O_2 staging. These yield enhancements exceed those achieved with previously reported three-stage reactor systems. The O_2 staging approach reported here requires only one reactor and one catalytic composition; thus, it decreases significantly process complexity and cost. H_2 removal by selective combustion using O_2 requires precise control of O_2 introduction and availability in order to avoid H_2 depletion and high CO selectivities, which can lead to unreactive deposits and to catalyst deactivation during alkane dehydrogenation.

1. Introduction

The selective conversion of light alkanes to alkenes provides an attractive route to useful chemicals [1]. Several alkane dehydrogenation processes [2–6] use supported Cr oxide catalysts. Recently developed dehydrogenation processes are based on supported Pt catalysts [2–6]. Both Pt and Cr catalysts deactivate rapidly and require frequent oxidative regenerations, which increase process complexity and capital and operating costs. Alkene yields are often limited by thermodynamics and the resulting low conversions introduce significant recycle and separation costs.

Dehydrogenation catalysts must increase the rate of desired reactions while minimizing side reactions, such as cracking, hydrogenolysis, oligomerization, cyclization, and aromatization, as well as the formation of unreactive carbon residues. Pt/Al_2O_3 is active in dehydrogenation reactions [1,7], but deactivates rapidly via formation of unsaturated organic residues. Pt clusters supported on Al_2O_3, SiO_2, ZrO_2 [7–9], L-zeolite [10], and $MgAl_2O_4$ [11] and modified with Sn give lower cracking, isomerization, and coke formation rates [1,12,13]. Sn and Pt appear to mix as small bimetallic clusters [14], which are better dispersed and more stable than Pt/γ-Al_2O_3 [7], but C_3H_8 dehydrogenation rates (30 kPa, 792 K) still decrease rapidly during reaction.

High H_2 concentrations limit alkene product yields by increasing the rate of the reverse reactions. In contrast, alkene yields are not thermodynamically limited in oxidative dehydrogenation reactions, because H-atoms formed in C–H bond activation steps are directly removed as H_2O. Alkene yields in oxidative dehydrogenation reactions are limited, however, by parallel and sequential oxidation reactions to form CO and CO_2 [15–21]. Thermodynamic constraints in

* Corresponding author.
E-mail address: iglesia@cchem.berkeley.edu (E. Iglesia).
[1] Permanent address: Central Technical Research Laboratory, Nippon Oil Corporation, Yokohama 231-0815, Japan.

0021-9517/$ – see front matter
doi:10.1016/j.jcat.2003.12.011

alkane dehydrogenation can be removed by continuously removing H_2 using membranes [22,23] or selective reactions with coreactants, such as O_2 [24,25]. The latter approach differs mechanistically from oxidative dehydrogenation, because H_2 reacts with O_2 after it desorbs, possibly on sites different from those used in dehydrogenation steps.

Here, we report a novel alkane dehydrogenation catalyst prepared by exchange of small amounts of Pt (0.1 wt% Pt) onto Na-[Fe]ZSM5 [26]. These materials give high C_3H_6 selectivity (> 97%), very high reaction rates, near-equilibrium alkene yields, and unprecedented stability. Deactivation rate constants are more than 10 times smaller than on previously reported Pt–Sn catalysts [7]. Staged introduction of O_2 coreactants during C_2H_6 and C_3H_8 dehydrogenation led to selective combustion of H_2 products and to the substantial removal of thermodynamic constraints.

2. Experimental methods

2.1. Catalyst synthesis and characterization

Na-[Fe]ZSM5 was prepared using methods previously described [27]. [Fe]ZSM5 was treated in flowing dry air (0.4 $cm^3/(g\,s)$) at 723 K for 15 h to remove organic templates used in its synthesis. This sample was exchanged three times with a $NaNO_3$ solution (Fisher, Certified ACS, > 98.0%, 0.5 liter/g-zeolite of a 2 g/liter $NaNO_3$ solution) at 353 K for 15 h and then filtered and washed with deionized water (2 liter/g ZSM5) to obtain Na-[Fe]ZSM5. Na-[Fe]ZSM5 was treated in flowing dry air (0.4 $cm^3/(g\,s)$) at 723 K for 15 h in order to remove residual nitrates. Pt cations were introduced by ion exchange with 0.001 M $Pt(NH_4)_4(NO_3)_2$ (Johnson Matthey/Aesar) for 12 h at 353 K. Exchanged samples were filtered, washed with deionized water, and treated in flowing dry air (0.4 $cm^3/(g\,s)$) at 723 K for 12 h. Si, Fe, and Pt contents were measured by atomic emission methods; they were 0.10 wt%. Pt and 0.44 wt% Fe$\{(Si/Fe)_{at} = 200\}$. Al was present in trace amounts (0.03 wt%). The fractional Pt dispersion was 0.95; it was obtained from the uptake of strongly chemisorbed hydrogen at 293 K, after samples were dried in He (0.5 $cm^3/(g\,s)$) at 573 K for 1 h and reduced at 573 K in H_2 (0.5 $cm^3/(g\,s)$) for 2 h.

2.2. Catalytic reaction rates and selectivities

Reaction rates and selectivities were measured using a packed-bed with plug-flow hydrodynamics and a gradientless recirculating reactor operated in either batch or semibatch mode [28]. In plug-flow mode, rate data were obtained at 793 K, 25 kPa C_3H_8/He (Praxair, certified mixture), and 4.1–78.7 mol C_3H_8/(g-atom Pt s) space velocities. Catalysts (0.03 g) were treated in 40% H_2/He (Airgas, UHP, 10 $cm^3/(g\,s)$) at 773 K before rate measurements.

In recirculating mode, rates were measured for C_3H_8 (5 or 20 kPa, Praxair) at 723 K and for C_2H_6 (20 kPa, Scott Specialty Gases, Inc.) at 773 K using the following protocols:

(i) *Pure alkane reactants*.
(ii) *Staged feed mode*: Alkanes were introduced at the start of each experiment and O_2 (Scott Specialty Gases, 99.999%) was added continuously using a 60-m quartz capillary (HP, 0.25-mm diameter). O_2 introduction rates (0.053–0.28 mol/(g-atom Pt s)) were chosen based on average H_2 formation rates during alkane reactions (without O_2); they were controlled by varying upstream capillary pressures; the O_2 staging protocols used are described in Table 1.
(iii) *Cofeed mode*: C_3H_8 (20 kPa, Praxair, CP) and O_2 (4 kPa) (Scott Specialty Gases, Inc., 99.999%) were concurrently added at the start of experiment.

O_2 staging intensities are defined as O_2 introduction rates divided by the corresponding rates required to consume all H_2 formed during an equivalent O_2-free alkane dehydrogenation experiment, if O_2 molecules were introduced at a uniform rate during staged O_2 experiments. A staging intensity of unity corresponds to O_2 addition rates of 0.16 mol/(g-atom Pt s) for 20 kPa C_3H_8 reactants at 723 K, 0.050 mol/g-atom Pt s) for 5 kPa C_3H_8 at 723 K, and 0.14 mol/(g-atom Pt s) for 20 kPa C_2H_6 at 773 K. These O_2 introduction rates would lead to the ultimate consumption of all H_2 produced during each experiment, when O_2 is used only to form H_2O and when the amounts of alkenes and H_2 produced are similar in O_2-free and staged O_2 experiments. Both assumptions represent approximations, but staging intensities remain a useful descriptive measure of O_2 introduction rates.

Reactants were introduced into the recirculating reactor volume (520 cm^3) after evacuation to < 0.1 Pa. A graphite gear pump was used to circulate reactor con-

Table 1
O_2 staging protocols during alkane dehydrogenation reactions on 0.1 wt% Pt/Na-[Fe]ZSM5 in a gradientless batch reactor

(a) 20 kPa C_3H_8 at 723 K	Contact time (ks)	0–0.3	0.3–2.4	2.4–6.6
	O_2 introduction rate (mol/(g-atom Pt s))	0	0.23	0.14
(b) 5 kPa C_3H_8 at 723 K	Contact time (ks)	0–0.3	0.3–6.2	–
	O_2 introduction rate (mol/(g-atom Pt s))	0	0.053	–
(c) 20 kPa C_2H_6 at 773 K	Contact time (ks)	0–0.3	0.3–0.7	0.7–4.3
	O_2 introduction rate (mol/(g-atom Pt s))	0	0.28	0.14

tents at > 2 cm^3/s in order to ensure gradientless operation ($< 1\%$ alkane conversion per pass). Catalysts were treated in 40% H_2/He (Airgas, UHP, 10 cm^3/(g s)) at 773 K for 1 h before reaction. During the initial stages of reaction (0.5–1.0 h) alkene selectivities increased because of selective deactivation of acid sites that formed C_1 and C_2 products. Therefore, samples were exposed to C_3H_8 at 773 K and 18.6 mol C_3H_8/(g-atom Pt s) space velocity for 2 h in continuous flow mode before batch or semibatch mode experiments in order to ensure steady-state catalytic rates and selectivities. Reactant and product concentrations were measured by on-line gas chromatography (Hewlett Packard, Model 5890) using capillary (HP-1 methyl silicone column, 50 m, 320 μm) and packed (Supelco, 1000 Carboxen) columns and flame ionization and thermal conductivity detectors. Samples were collected using a valve located within the recirculation loop.

Plug-flow reactor rates are reported as moles of reactant consumed or product formed per g-atom Pt-s. Product concentrations in recirculating modes are given as site yields [(moles of reactant converted to a given product)/(g-atom Pt)]; the slope of such plots gives reaction rates in terms similar to those used for flow reactor data. Hydrocarbon selectivities are reported on a carbon basis as the percentage of the converted reactant appearing as a given reaction product. Oxygen selectivities are also reported for O_2 introduction experiments; they are defined as the percentage of the O_2 introduced that is used for H_2 combustion to form H_2O or for hydrocarbon combustion to form CO_x (CO and CO_2) and the stoichiometric amount of H_2O.

Lund and co-workers [29] previously described a mathematical analogy between H_2 removal during dehydrogenation reactions in batch and flow membrane reactors. A similar analysis supports a rigorous mathematical analogy between semibatch reactors with continuous O_2 feed and plug-flow reactors with multiple axial injection points (or O_2-permeable walls) [30]. Thus, the continuous O_2 introduction experiments described here provide a rigorous description of the effects of O_2 introduction along tubular dehydrogenation reactors.

The influence of reverse reactions on measured alkane dehydrogenation rates must be taken into account, especially as the reaction approaches equilibrium, in order to determine kinetically relevant forward reaction rates. The approach to equilibrium (η) depends on thermodynamic data and on the prevalent pressures of reactants and products:

$$C_3H_8 \rightarrow C_3H_6 + H_2,$$
$$\eta = \frac{[P_{C_3H_6}][P_{H_2}]}{[P_{C_3H_8}]} \times \frac{1}{K_{EQ}}. \quad (1)$$

The equilibrium constant K_{EQ} was obtained from literature data [31]. The value of $(1-\eta)$ represents the fractional distance from equilibrium. Net reaction rates can then be rigorously expressed as

$$r_{net} = r_{forward}(1-\eta), \quad (2)$$

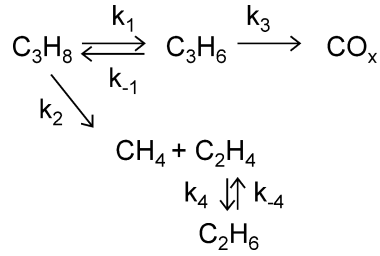

Scheme 1. C_3H_8 reaction pathways on Pt/Na-[Fe]ZSM5.

from which forward rates can be obtained:

$$r_{forward} = r_{net}/(1-\eta). \quad (3)$$

The effects of contact time of C_3H_8 dehydrogenation rates were described using the set of reactions shown in Scheme 1. Rate and selectivity data were used to estimate each rate constant assuming pseudo-first-order kinetics for forward reactions and thermodynamic relations for all reverse rate constants. The linear set of differential equations was solved using known methods [32]; a regression analysis was used to minimize deviations between model predictions and experimental data.

3. Results and discussion

3.1. C_3H_8 dehydrogenation reactions on Pt/Na-[Fe]ZSM5 in a packed-bed plug-flow reactor

C_3H_8 dehydrogenation rates and selectivities were measured on 0.1 wt% Pt/Na-[Fe]ZSM5 catalyst at 793 K, 25 kPa C_3H_8, and 4.1–78.7 mol C_3H_8/(g-atom Pt s) space velocity in a plug-flow reactor (Table 2). The equilibrium conversion of C_3H_8 to C_3H_6 under these conditions is $\sim 36\%$. This catalyst led to near-equilibrium C_3H_6 yields (35%) with 97% C_3H_6 selectivity, and a net C_3H_6 formation turnover rate of 1.4 mol C_3H_8/(g-atom Pt s) at 4.1 mol C_3H_8/(g-atom Pt s) space velocity. These net rates are similar to those reported (1.1 mol C_3H_8/(g-atom Pt s)) at 792 K and slightly lower space velocities (3.5 mol C_3H_8/(g-atom Pt s)) on 0.35 wt% Pt–Sn/γ-Al_2O_3; these previously reported rates, however, decreased rapidly with time on stream [7]. Measured C_3H_6 formation rates on 0.1 wt%. Pt/Na-[Fe]ZSM5 decreased with increasing residence time (Table 2, Fig. 1), as the dehydrogenation reaction approached equilibrium. The effects of residence time on forward reaction rates, obtained from the measured net rates using Eq. (3), are much weaker (Fig. 1); they merely reflect C_3H_8 depletion by reaction and the observed first-order dependence of forward dehydrogenation rates on C_3H_8 pressure.

C_3H_6 selectivities decreased slightly with increasing residence time, because hydrogenolysis and cracking remained far from equilibrium as dehydrogenation reactions approached equilibrium with increasing residence time. Even at C_3H_8 conversions near equilibrium ($\sim 35\%$), C_3H_6

Table 2
C_3H_8 dehydrogenation turnover rates and product distribution in a packed-bed plug-flow reactor [793 K, 25 kPa C_3H_8, balance He, 0.1 wt% Pt/Na-[Fe]ZSM5]

Space velocity (mol C_3H_8/(g-atom Pt s))	4.1	8.1	16.2	31.5	78.7
C_3H_8 conversion (%)	35.5	33.7	31.2	27.4	18.9
Carbon selectivity (%)					
CH_4	0.68	0.42	0.18	0.14	0.10
C_2H_4	0.13	0.07	0.05	0.05	0.05
C_2H_6	1.32	0.65	0.34	0.24	0.14
C_3H_6	96.9	98.2	98.9	99.2	99.6
Others (C_{4+})	0.97	0.65	0.53	0.37	0.07
Molar ratio of (C_2H_4/C_2H_6)	0.10	0.11	0.13	0.18	0.31
Molar ratio of (C_2H_4/C_2H_6) at equilibrium	0.080	0.082	0.088	0.10	0.14
$\eta(C_3H_8 \rightarrow C_3H_6 + H_2)$	0.91	0.83	0.70	0.52	0.23
Net C_3H_6 formation turnover rate (mol/(g-atom Pt s))	1.42	2.67	5.00	8.55	14.8
Forward C_3H_6 formation turnover rate (mol/(g-atom Pt s))[a]	15.7	16.0	16.7	17.8	19.2

[a] Calculated from net rate and η using Eq. (3).

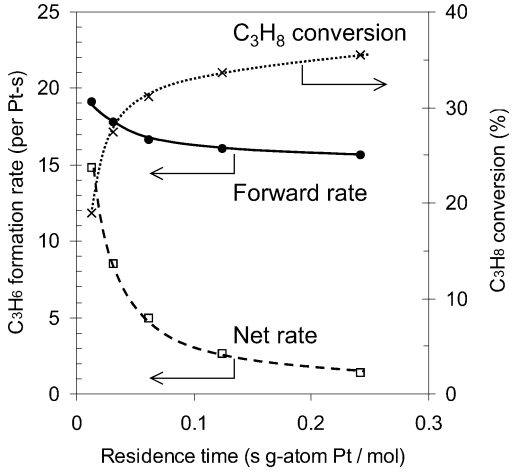

Fig. 1. C_3H_8 conversion and net and forward C_3H_6 formation rates during C_3H_8 dehydrogenation reactions in a packed-bed plug-flow reactor [793 K, 25 kPa C_3H_8, 4.1–78.7 mol C_3H_8/(g-atom Pt s), balance He, 0.1 wt% Pt/Na-[Fe]ZSM5].

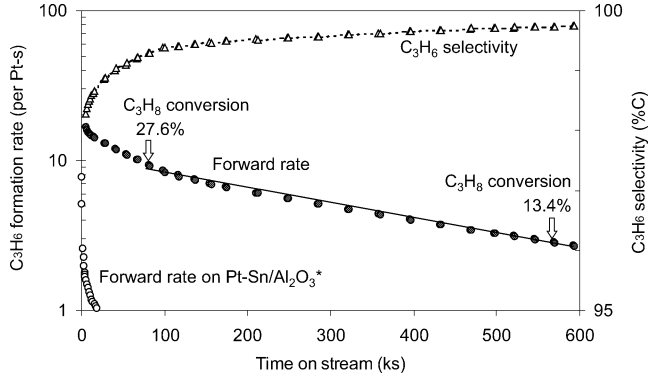

Fig. 2. Forward C_3H_6 formation rates and C_3H_6 selectivities during C_3H_8 dehydrogenation reactions [793 K, 25 kPa C_3H_8, 18.6 mol C_3H_8/(g-atom Pt s), balance He, 0.1 wt% Pt/Na-[Fe]ZSM5, packed-bed flow reactor].
*Calculated using Eq. (3) from the net rates on the 0.35 wt%. Pt–Sn/γ-Al_2O_3 at 30 kPa C_3H_8, 3.5 mol C_3H_8/(g-atom Pt s), and 792 K reported in [7].

selectivities were very high (97%), as also found on Pt–Sn/γ-Al_2O_3 (95–98%) [7]. C_2H_4/C_2H_6 ratios were higher than thermodynamic values and decreased with increasing residence time (Table 2); these data indicate that C_2H_6 forms via hydrogenation of C_2H_4 formed in primary cracking reactions. Direct formation of C_2H_6 via hydrogenolysis of C_3H_8 was not detected, consistent with the structure sensitivity of these reactions and the low turnover rates reported on highly dispersed Pt clusters [33]. Only traces of C_6–C_8 aromatics ($< 1\%$ selectivity) were detected, suggesting that residual acid sites (formed during reduction of exchanged Pt cations) are relatively inactive in oligomerization and cyclization reactions, because of their weak acidity in [Fe]ZSM5 or their rapid deactivation during the early stages of reaction (Table 2). In contrast, such chain growth and cyclization reactions are very fast during C_3H_8 reactions on H-[Al]ZSM5 and cation-exchanged H-[Al]ZSM5 [34,35].

C_3H_8 dehydrogenation rates were measured after H_2 treatment for 3 h on 0.1 wt% Pt/Na-[Fe]ZSM5 at 793 K and 18.6 mol C_3H_8/(g-atom Pt s) space velocity for 160 h in a packed-bed flow reactor (Fig. 2). C_3H_6 selectivities increased sharply during initial contact with reactants (~ 100 ks) and then gradually at longer times (98.3 to 99.8%), until other products became nearly undetectable (Fig. 2); these findings appear to reflect the selective deactivation of acid sites responsible for cracking reactions. Concurrently, net dehydrogenation rates decreased from 5.9 to 2.7 mol C_3H_8/(g-atom Pt s) over ~ 160 h, corresponding to a decrease in forward reaction rate from 16.7 to 3.0 mol C_3H_8/(g-atom Pt s) (Fig. 2). Shorter H_2 treatments (1 h) before reaction led to incomplete reduction of Pt/Na-[Fe]ZSM5 and to a gradual initial increase in dehydrogenation rates as reduction continued during initial contact with C_3H_8 reactants.

Deactivation rates were much lower on 0.1 wt% Pt/Na-[Fe]ZSM5 at 793 K than on 0.35 wt% Pt–Sn/γ-Al_2O_3, on which net C_3H_6 formation rate decreased by a factor of about 2 in ~ 10 h at 792 K [7]. In order to measure deactivation rate constants rigorously, forward reaction rates were es-

timated on 0.1 wt% Pt/Na-[Fe]ZSM5 using the data reported here and on 0.35 wt% Pt–Sn/γ-Al_2O_3 using reported net rates [7] and Eq. (3). Deactivation rate constants decreased rapidly during the early stages of reaction on both catalysts (Fig. 2), apparently because alkene and acid site concentrations decreased as deactivation occurred. First-order deactivation constants then reached constant values (Fig. 2) of 0.008 h^{-1} on Pt/Na-[Fe]ZSM5 (80–600 ks) and 0.11 h^{-1} on Pt–Sn/γ-Al_2O_3 (6–18 ks). These rate constants correspond to mean lives (τ; defined as the time required for the rate to reach e^{-1} of its initial value) of $\sim$ 125 h on Pt/Na-[Fe]ZSM5 and $\sim$ 9 h on Pt–Sn/γ-Al_2O_3. The isomorphic substitution of Al^{3+} by Fe^{3+} in ZSM5 leads to weaker acidity [36], while the presence of small Pt clusters within protected 10-ring channels leads, in turn, to low hydrogenolysis turnover rates and to constrained environments that preclude transition states required to form large organic structures. These combined effects led to lower rates of oligomerization, cyclization, and aromatization and to an apparent decrease in the rate of formation of unreactive organic residues responsible for deactivation on Pt/Na[Fe]ZSM5 catalysts.

After C_3H_8 reactions for 160 h, Pt/Na-[Fe]ZSM5 was treated in a flowing 40% H_2 in He (10 $cm^3/(g\,s)$) mixture at 773 K for 2 h. This treatment did not recover or even influence dehydrogenation rates, indicating that organic residues responsible for deactivation do not react with H_2 at reaction temperatures. Treatment in 1% O_2/He (10 $cm^3/(g\,s)$) at 723 K for 2 h and re-reduction of the catalyst in a flowing 40% H_2 in He (10 $cm^3/(g\,s)$) mixture at 773 K for 2 h, however, led to initial forward C_3H_8 dehydrogenation rates (16.1 mol C_3H_8/(g-atom Pt s)), very similar to those on fresh catalysts (16.7 mol C_3H_8/(g-atom Pt s)). Deactivation rate constants (0.009 h^{-1}) and C_3H_6 selectivities (99.6% after 50 h) were nearly identical to those on fresh catalysts (0.008 h^{-1}, 99.4%). We conclude that oxidative treatments remove organic residues without any sintering or migration of Pt clusters. The deposition of organic residues is responsible for the slow deactivation observed during C_3H_8 dehydrogenation on Pt/Na-[Fe]ZSM5; such residues can be fully removed, however, using mild oxidative treatments.

3.2. Comparison of Pt/Na-[Fe]ZSM5 with previously reported alkane dehydrogenation catalysts

Pt and Pt–Sn species on nonacidic supports, such as $MgAl_2O_4$, lead to lower cracking and oligomerization rates and to slower deactivation than similar active structures supported on γ-Al_2O_3 or SiO_2 [11,37]. C_3H_8 dehydrogenation on 0.5 wt% Pt–Sn/$MgAl_2O_4$ at 823 K, 39 kPa, and a space velocity of 9 mol C_3H_8/(g-atom Pt s) led to 93–97% C_3H_6 selectivity and 11–12% C_3H_8 conversion [11]. Deactivation rate constants obtained from forward reaction rates (0.05 h^{-1}) were lower than on Pt–Sn/γ-Al_2O_3 (0.11 h^{-1}) [7], but much greater than reported here on Pt/Na-[Fe]ZSM5 (0.008 h^{-1}). Pt–Ga/$MgAl_2O_4$ shows greater rates, selectivity, and stability than Pt–Sn/$MgAl_2O_4$ [38]. C_3H_8 reactions on 0.6 wt% Pt–Ga/$MgAl_2O_4$ at 878 K, 78 kPa, and 0.80 mol C_3H_8/(g-atom Pt s) space velocity led to $\sim$ 30% conversion and 97–98% C_3H_6 selectivity, but deactivation rate constants ($\sim$ 0.05 h^{-1}) were also much higher than on Pt/Na-[Fe]ZSM5.

Pt clusters on silicalite (pure silica ZSM5) also catalyze alkane dehydrogenation with high selectivity [39], but reaction rates are much lower than on Pt/Na-[Fe]ZSM5, apparently because the absence of exchange sites in silicalite leads to low dispersion of Pt precursors and crystallites. Deactivation rates are much lower than on Pt/Al_2O_3 and the addition of Zn increases rates, selectivity, and stability [40]. C_3H_8 reactions on 0.5 wt% Pt/Zn/silicalite at 828 K and 0.7 mol C_3H_8/(g-atom Pt s) space velocity led to 25–27% C_3H_8 conversion with 99% C_3H_6 selectivity; deactivation rate constants ($\sim$ 0.01 h^{-1}) are slightly higher than reported here on 0.1 wt% Pt/Na-[Fe]ZSM5, which gives higher C_3H_6 yields (35%) at higher space velocities (4.1 mol C_3H_8/(g-atom Pt s) and lower temperatures (793 K) than these state-of-the-art Pt-based silicalite materials.

3.3. Effects of H_2 removal by staged O_2 introduction in a gradientless batch reactor

Thermodynamic constraints imposed by increasing H_2 concentrations as alkane conversion increases prevent the use of these active and stable catalysts at even lower temperatures or higher conversions. In principle, these constraints can be removed by reactions that consume H_2 as it forms. In practice, this requires that coreactants interact selectively with H_2, without significant depletion of hydrocarbon reactants or products. For example, H_2 combustion with O_2 effectively removes H_2, but the combustion of the predominant alkanes and alkenes must be much slower than the desired combustion of H_2. H_2 combustion selectivity should be favored when O_2 is not available before H_2 is formed or after H_2 is depleted. The concurrent introduction of O_2 and alkanes in the reactant stream can lead to significant hydrocarbon combustion before H_2 becomes available from dehydrogenation reactions. Here, we explore the kinetic and thermodynamic consequences of staging the introduction of O_2 coreactants as alkane conversion proceeds and H_2 becomes available for reaction with O_2.

Previous studies of O_2 staging during C_3H_8 dehydrocyclodimerization reactions on cation-exchanged H-[Al]ZSM5 [41] led to significant increases in aromatic yields over those achieved with pure C_3H_8 reactants. Staging intensities above stoichiometric values led to lower O_2 reactant efficiencies without significant additional improvements in aromatic yields beyond those obtained at staging intensities near unity [41]. Therefore, O_2 introduction rates corresponding to overall staging intensities near unity were chosen initially for C_3H_8 and C_2H_6 reactions on 0.1 wt% Pt/Na-[Fe]ZSM5. O_2 introduction rates that vary with time, so as to more closely match the higher initial H_2 formation rates and their ultimate decrease as conversion increases, ulti-

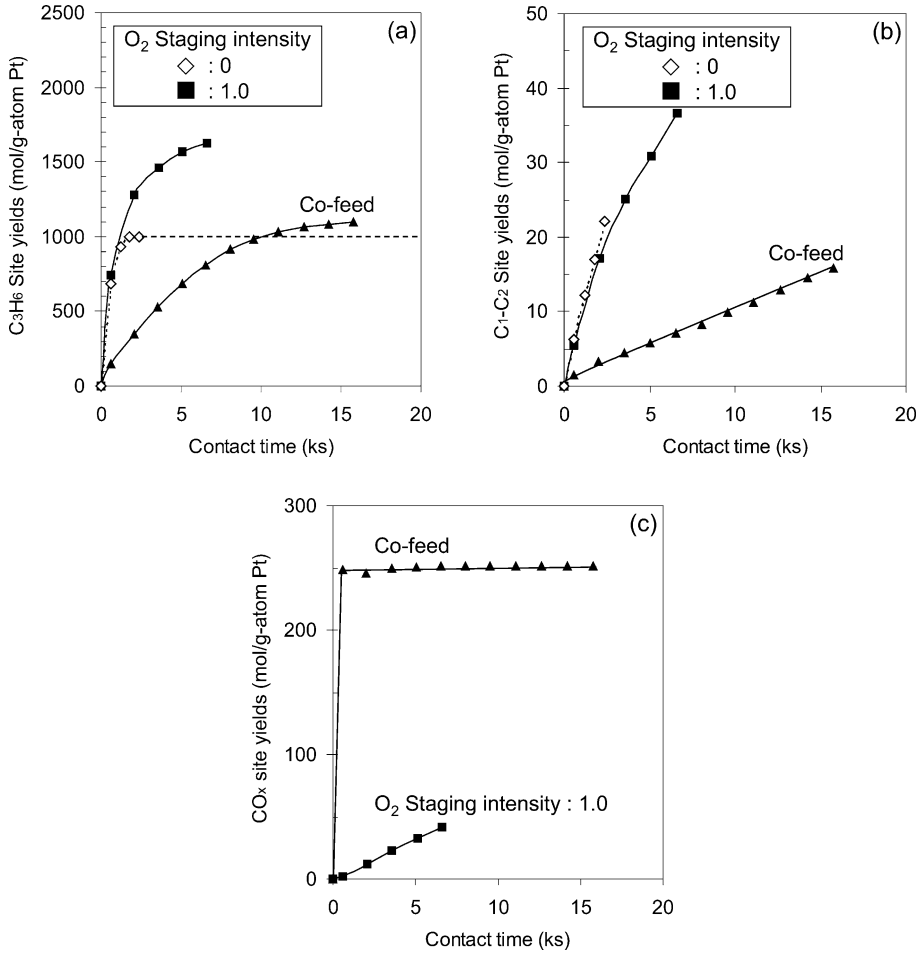

Fig. 3. Effects of O_2 introduction on (a) C_3H_6, (b) cracking products (C_1–C_2), and (c) carbon oxide (CO_x) site yields during C_3H_8 dehydrogenation reactions in a gradientless batch reactor [723 K, 20 kPa C_3H_8, cofeed: 4 kPa O_2 or O_2 staging protocol: (1) 0–0.3 ks without O_2, (2) 0.3–2.4 ks 0.23 mol/(g-atom Pt s) (3) 2.4–6.6 ks 0.14 mol/(g-atom Pt s), balance He, 0.1 wt% Pt/Na-[Fe]ZSM5].

mately led to more precise matching of O_2 introduction and H_2 formation rates and they were used in all experiments reported here. For C_3H_8 dehydrogenation, O_2 introduction protocols that maintain an overall staging intensity of unity were implemented by initially using pure C_3H_8 for 0.3 ks in the batch recirculating reactors; O_2 was then added at 0.23 mol/(g-atom Pt s) between 0.3 and 2.4 ks and finally at 0.14 mol/(g-atom Pt s) from 2.4 to 6.6 ks (Table 1a).

Fig. 3 shows site yields for C_3H_6, C_1–C_2, and carbon oxide (CO_x) product yields during C_3H_8 dehydrogenation at 723 K and 20 kPa C_3H_8 in a gradientless batch reactor. Equilibrium C_3H_6 yields were quickly reached and C_3H_6 (Fig. 3a) and H_2 (Fig. 4a) site yields reached constant values ($\sim 10^3$ mol/g-atom Pt) after 2.4 ks. C_3H_6 formation rates decreased with increasing contact time (Fig. 3a), because H_2 accumulates as conversion increases. H_2 increases the rate of reverse reactions and can also inhibit forward dehydrogenation rates.

Higher C_3H_6 yields were achieved when O_2 was introduced gradually during reaction (Fig. 3a). Maximum C_3H_6 site yields increased from $\sim 10^3$ mol C_3H_6/g-atom Pt (18% yield) to $\sim 1.7 \times 10^3$ mol C_3H_6/g-atom Pt (29% yield) when O_2 was introduced at overall staging efficiencies of unity on Pt/Na-[Fe]ZSM5. C_3H_6 formation rates decreased with increasing contact time during staging experiments (Fig. 3a), as H_2 was nearly depleted via reactions with O_2 (Fig. 4a). This reflects higher deactivation rates as H_2 concentrations decrease and catalysts are exposed to higher concentrations of CO and alkenes without the concurrent presence of H_2. Such conditions favor larger and less reactive unsaturated products and the formation of adsorbed carbon species via CO disproportionation reactions. These deactivation processes will be discussed in more detail in a later section. Cracking (C_1–C_2) rates were not influenced by the presence of O_2 coreactants or by the removal of H_2 (Fig. 4b), because cracking reactions remained far from equilibrium under all reaction conditions.

C_2H_4/C_2H_6 molar ratios were higher than equilibrium values at all contact times with pure C_3H_8 reactants and during O_2 staging (Table 3), indicating that C_2H_4 is formed in primary cracking reactions of C_3H_8; C_2H_6 is formed via secondary hydrogenation of C_2H_4 and not via direct hy-

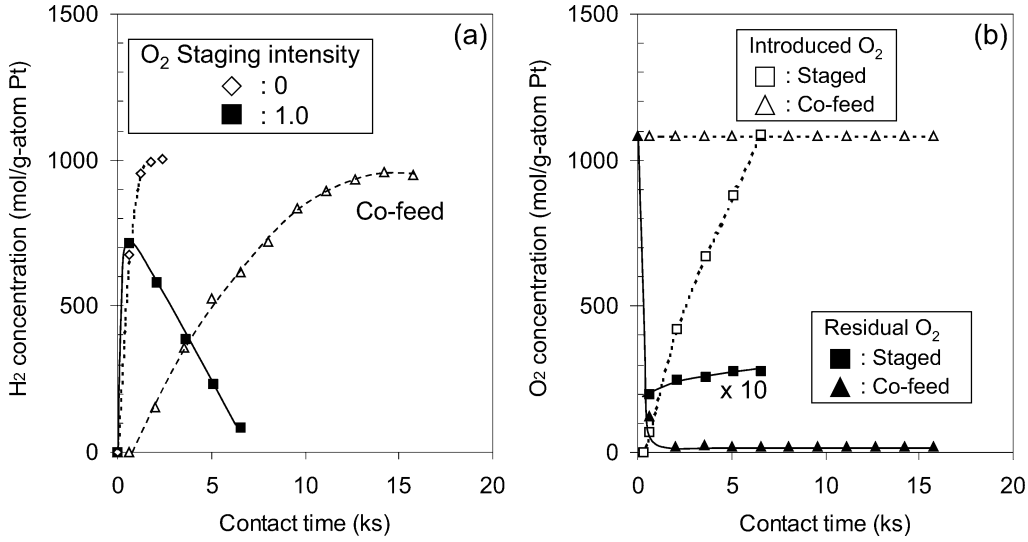

Fig. 4. (a) Hydrogen concentrations and (b) total amounts of introduced O_2 and residual O_2 concentrations during C_3H_8 dehydrogenation reactions in a gradientless batch reactor [723 K, 20 kPa C_3H_8, cofeed: 4 kPa O_2 or O_2 staging protocol: (1) 0–0.3 ks without O_2, (2) 0.3–2.4 ks 0.23 mol/(g-atom Pt s), (3) 2.4–6.6 ks 0.14 mol/(g-atom Pt s), balance He, 0.1 wt% Pt/Na-[Fe]ZSM5].

Table 3
Effects of O_2 staging on ratios of C_2H_4 to C_2H_6 during C_3H_8 dehydrogenation reaction in a packed-bed flow reactor [723 K, 20 kPa C_3H_8, O_2 staging protocol: (1) 0–0.3 ks without O_2, (2) 0.3–2.4 ks 0.23 mol/(g-atom Pt s), (3) 2.4–6.6 ks 0.14 mol/(g-atom Pt s), balance He, 0.1 wt% Pt/Na-[Fe]ZSM5]

O_2 staging intensity	0	0	0	1.0	1.0	1.0
Contact time (ks)	0.6	1.2	2.4	0.6	3.6	6.6
C_3H_8 conversion to hydrocarbons (%)	12.5	17.1	18.4	13.3	26.5	29.7
H_2 site yields (mol/g-atom Pt)	680	950	1000	580	390	85
Molar ratio of (C_2H_4/C_2H_6)	0.26	0.16	0.091	0.28	0.38	0.75
Molar ratio of (C_2H_4/C_2H_6) at equilibrium	0.12	0.089	0.083	0.17	0.26	0.75
$\eta(C_2H_4 + H_2 \rightarrow C_2H_6)$	0.48	0.54	0.91	0.60	0.67	0.84

drogenolysis of C_3H_8 on Pt clusters. C_2H_4/C_2H_6 ratios decreased with increasing contact time for O_2-free reactants, but increased during O_2 staging, because C_2H_4 hydrogenation reactions depend on H_2 concentrations. H_2 concentrations decreased with contact time in staging experiments but increased during reactions of pure C_3H_8 reactants (Table 3). For both pure C_3H_8 reactants and staged O_2 introduction experiments, the reaction equilibrium parameter η for C_2H_4 hydrogenation approached unity with increasing contact time (Table 3).

The percentage of the converted O_2 used for H_2 combustion reflects the relative reactivity and availability of H_2, alkanes, and alkenes for reactions with O_2. Fig. 4b shows added and residual amounts of O_2 during C_3H_8 reactions on Pt/Na-[Fe]ZSM5 at 723 K. Residual O_2 concentrations are very low (< 0.1 μmol/cm^3) throughout the entire conversion and contact time range. Fig. 5 shows that 89–93% of the added O_2 is used to combust H_2, indicating that H_2 removal by O_2 is very selective when O_2 coreactants are staged in a manner that ensures that H_2 is available as O_2 coreactants enter the reacting mixture. These H_2 combustion selectivities are remarkable in view of the predominant presence of hydrocarbons in the prevalent reacting mixtures.

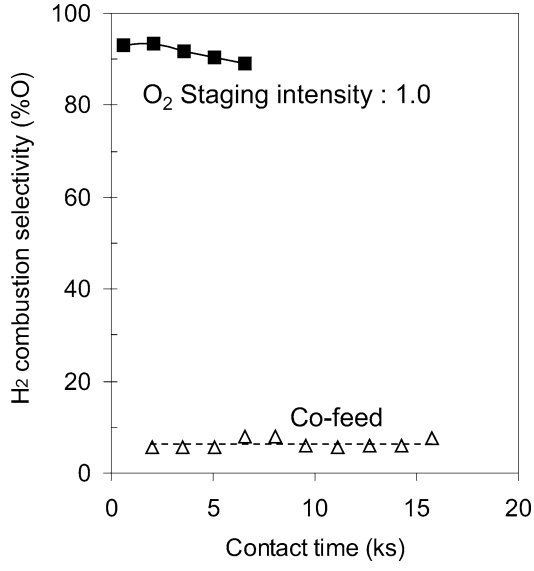

Fig. 5. H_2 combustion selectivities (% O-base) in cofeed and staged modes during C_3H_8 dehydrogenation reactions in a gradientless batch reactor [723 K, 20 kPa C_3H_8, cofeed: 4 kPa O_2 or O_2 staging protocol: (1) 0–0.3 ks without O_2, (2) 0.3–2.4 ks 0.23 mol/(g-atom Pt s), (3) 2.4–6.6 ks 0.14 mol/(g-atom Pt s), balance He, 0.1 wt% Pt/Na-[Fe]ZSM5].

In order to determine the extent to which homogeneous reactions contribute to combustion pathways, the reaction products and unreacted C_3H_8 remaining after C_3H_8 reactions on Pt/Na-[Fe]ZSM5 (17% conversion; 3.6 ks, 723 K) were isolated, mixed with 1 kPa O_2, and reacted in an empty reactor at 723 K (0.7 cm^3 heated volume). CO_x formation and H_2 combustion rates were compared at similar H_2 and O_2 concentrations with those measured during catalytic dehydrogenation reactions using the O_2 introduction protocol described in Table 1a. Catalytic CO_x formation and H_2 combustion rates were much higher than homogeneous rates (Table 4), indicating that observed alkene and H_2 combustion rates during staged and cofeed O_2 experiments reflect surface-catalyzed reactions. Homogeneous first-order combustion rate constants were about 15 times greater for C_3H_6 than for C_3H_8; taken together with the low initial CO_x selectivity in catalytic staged experiments and its increase with contact time, these data suggest that CO_x formed during staging catalytic experiments arise predominately from combustion reactions of alkenes formed in dehydrogenation reactions.

Table 4
C_3H_8 to CO_x turnover rates on 1.0% Pt/Na-[Fe]ZSM5 and in an empty reactor [catalytic reaction: 723 K, 20 kPa C_3H_8, 0.23 mol/(g-atom Pt s) O_2, balance He, 1.0% Pt/Na-[Fe]ZSM5; homogeneous reaction: 723 K, reactant and products after the catalytic reaction for 1 h (723 K, 20 kPa C_3H_8, balance He), 1 kPa O_2, empty reactor]

	Pt/Na-[Fe]ZSM5	Homogeneous
Carbon oxide formation rate (mol/cm^3, 10^{-13} s^{-1})	300	4.6
H_2 combustion rate (mol/cm^3, 10^{-12} s^{-1})	660	7.3
Residual H_2 concentration (mol/cm^3, 10^{-7})	9.2	9.0
Residual O_2 concentration (mol/cm^3, 10^{-8})	2.5	2.4

O_2 staging experiments were also carried out at lower initial C_3H_8 pressures (5 kPa) and overall O_2 staging intensities of unity (Table 5). The O_2 staging protocol is shown in Table 1b. Higher maximum C_3H_6 yields were achieved with O_2 staging at 5 kPa (40.5%) than at 20 kPa (28.8%), but the ratios of these C_3H_6 yields to the corresponding equilibrium yields were lower at 5 kPa C_3H_8 (1.26) than at 20 kPa (1.58). Fig. 6 shows that H_2 combustion selectivities were very similar for these two reactant pressures (e.g., 89% at 20 kPa and 87% at 5 kPa and 30% conversion).

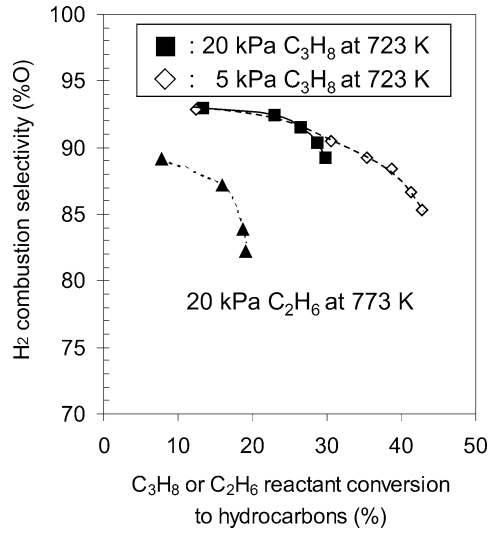

Fig. 6. H_2 combustion selectivities (% O-base) during alkane dehydrogenation reactions at O_2 staging intensities of 1.0 using staging protocols shown in Table 1 [20 kPa C_2H_6 and 5, 20 kPa C_3H_8, 0.1 wt% Pt/Na-[Fe]ZSM5, gradientless batch reactor].

Table 5
Comparison of dehydrogenation of light alkanes combined with selective hydrogen combustion [25] and with staged O_2 feed (this study)

Catalysts:	Catalytic dehydrogenation with staged O_2 feed: 0.1 wt% Pt/Na-[Fe]ZSM5			Three-stage dehydrogenation–selective hydrogen combustion [25]: 0.7 wt% Pt–Sn-ZSM5 (dehydrogenation sections) 10 wt% In_2O_3/ZrO_2 (selective hydrogen combustion sections)	
Reaction conditions					
Temperature (K)	723	723	773	823	823
Reactant	C_3H_8	C_3H_8	C_2H_6	C_3H_8	C_3H_8
Initial C_3H_8 (or C_2H_6) pressure (kPa)	20	5	20	101	101
Molar ratio of (introduced O_2/alkane)	0.14	0.20	0.10	0.06	0.12
C_3H_8 (or C_2H_6) conversion (% C)	30.5	43.2	20.4	30	35
C_3H_6 (or C_2H_4) selectivity (% C)	94.6	93.8	93.0	99	96
CO_x selectivity (% C)	2.4	3.0	5.0	1	4
H_2 combustion selectivity (% O)	89.2	85.3	80.3	–	–
C_3H_6 (or C_2H_4) yield (mol/g-atom Pt)	1600	590	1100	–	–
(% C)	28.8	40.5	18.9	30	33
C_3H_6 (or C_2H_4) yield at equilibrium (%, calculated)	18.2	32.2	12.0	25	25
Ratio of C_3H_6 (or C_2H_4) yield to C_3H_6 (or C_2H_4) yield at equilibrium	1.58	1.26	1.58	1.2	1.3

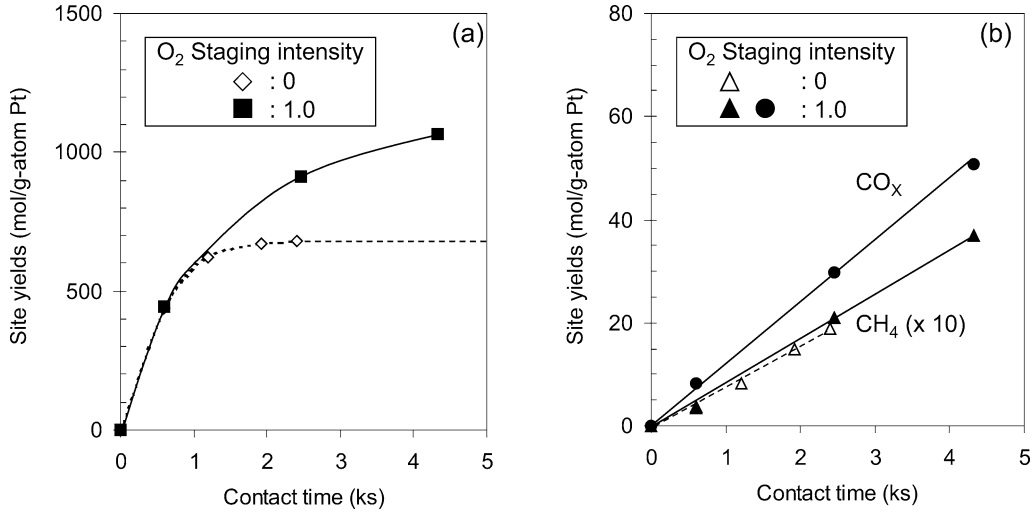

Fig. 7. Effects of O_2 staging on (a) C_2H_4, (b) CH_4, and carbon oxide (CO_x) site yields during C_2H_6 dehydrogenation reactions in a gradientless batch reactor [773 K, 20 kPa C_2H_6, O_2 staging protocol: (1) 0–0.3 ks without O_2, (2) 0.3–0.7 ks 0.28 mol/(g-atom Pt s), (3) 0.7–4.3 ks 0.14 mol/(g-atom Pt s), balance He, 0.1 wt% Pt/Na-[Fe]ZSM5].

C_2H_6 dehydrogenation (20 kPa) was also studied at 773 K on Pt/Na-[Fe]ZSM5 using the O_2 staging protocol shown in Table 1c. A higher temperature was chosen than that for C_3H_8 reactants because alkane reactivities and equilibrium alkene yields decrease with decreasing alkane chain size. C_2H_6 dehydrogenation data are shown in Fig. 7 and Table 5. Equilibrium C_2H_4 yields were quickly reached ($\sim$ 2 ks) with O_2-free reactants at 773 K. O_2 staging led to significantly higher yields (1.1×10^3 mol C_2H_4/g-atom Pt, 19% C_2H_4 yield) than with O_2-free reactants (0.68×10^3 mol C_2H_4/g-atom Pt, 12% C_2H_4 yield) (Fig. 7a). The ratio of the experimental to equilibrium C_2H_4 yields with O_2 staging was 1.58 (Table 5). H_2 combustion selectivities at similar alkane conversion levels were lower for C_2H_6 at 773 K than for C_3H_8 at 723 K (Fig. 6). This is not unexpected because H_2 combustion typically shows lower activation energies than hydrocarbon combustion reactions in homogeneous [42] and catalytic [43] systems. Thus, the higher reaction temperatures used in C_2H_6 dehydrogenation reactions favor combustion of the predominant hydrocarbon species over competing reactions of less abundant H_2 molecules.

3.4. Comparison of O_2 staging with cofeed strategies

C_3H_8 dehydrogenation rates and selectivities during staged O_2 introduction were compared with those measured when equivalent amounts of O_2 were introduced concurrently with C_3H_8 reactants. O_2 was introduced with C_3H_8 (20 kPa) either initially (4 kPa) or continuously (Table 1a; staging intensity of unity). In cofeed experiments, residual O_2 concentrations were initially very high, but O_2 was consumed rapidly in hydrocarbon combustion reactions to form CO_x and H_2O (Fig. 4b). O_2 became undetectable after $\sim$ 0.6 ks contact times, at which point C_3H_6 yields were still low (2.5%) and far from equilibrium; in cofeed experiments, O_2 was only available, and rapidly consumed in unselective hydrocarbon combustion reactions, when C_3H_8 conversions were low and H_2 was not yet available. As a result, O_2 was consumed unselectively and it became unavailable to remove H_2 as dehydrogenation reactions approached equilibrium. Fig. 3a also shows that C_3H_6 formation rates were much lower during cofeed experiments than in staged O_2 or O_2-free operating modes; this reflects deactivation events favored at the high CO concentrations and low H_2 concentrations prevalent during the early stages of C_3H_8 dehydrogenation with O_2 cofeed, as discussed below.

Fig. 3c shows CO_x site yields for stoichiometric staging and cofeed experiments. In cofeed mode, CO_x site yields initially increased rapidly with increasing contact time until O_2 was depleted and CO_x could no longer form. CO_x formation rates and site yields were much higher with C_3H_8–O_2 reactants than at the lower O_2 concentrations prevalent during staged O_2 introduction. H_2 combustion selectivities were much lower (5–8%) in cofeed experiments than during stoichiometric O_2 staging (90%) as shown in Fig. 5. The low H_2 combustion selectivities in cofeed experiments reflect the substantial absence of H_2 at short contact times, during which O_2 is abundant, and the depletion of O_2 via unselective reactions before dehydrogenation approaches equilibrium at longer contact times (Fig. 4b).

3.5. Catalyst deactivation during C_3H_8 dehydrogenation with O_2 introduction

When H_2 is removed selectively via reactions with O_2, alkene yields are no longer constrained by thermodynamics; as a result, they should increase monotonically with contact time. Near-stoichiometric O_2 introduction rates, however, led to asymptotic alkene yields as contact time increased (Fig. 3a, Fig. 7a). These data do not reflect any effects of reverse reactions, because H_2 was continuously removed as

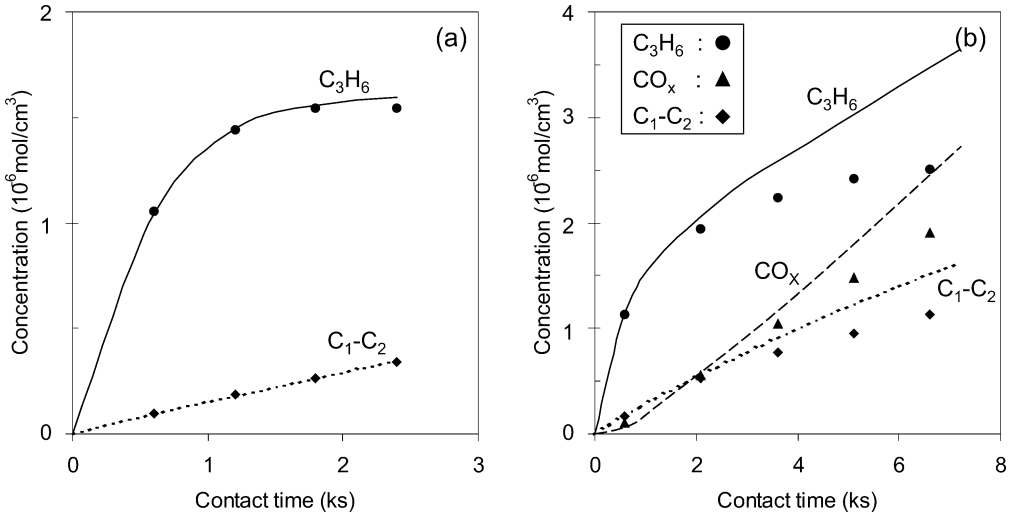

Fig. 8. Comparison of experimental concentrations (data points) of products to calculated or predicted concentrations from model (lines) (a) with O_2-free reactant (staging intensity = 0) and (b) with staged O_2 (staging intensity = 1.0) [723 K, 20 kPa C_3H_8, O_2 staging protocol: (1) 0–0.3 ks without O_2, (2) 0.3–2.4 ks 0.23 mol/(g-atom Pt s), (3) 2.4–6.6 ks 0.14 mol/(g-atom Pt s), balance He, 0.1 wt% Pt/Na-[Fe]ZSM5].

contact time increased via reactions with O_2 and its concentration remained very low. It is possible that H_2O or CO, formed in combustion reactions, inhibit or poison active sites, or that low H_2 concentrations prevalent during staging experiments favor unsaturated carbonaceous residues that block access to active sites. These possibilities were examined by comparing measured time yields with those predicted from thermodynamically consistent kinetic models of C_3H_6 dehydrogenation reactions.

On Pt/Na-[Fe]ZSM5, C_3H_8 reactions include primary dehydrogenation to form C_3H_6, primary cracking reactions to form CH_4 and C_2H_4 (Scheme 1), and secondary hydrogenation of C_2H_4 to form C_2H_6. Initial CO_x carbon selectivities (extrapolated to zero reactant conversion) are very low (< 0.1%), suggesting that CO_x forms predominately via combustion of C_3H_6 and not directly from C_3H_8. Rate constants for each nonoxidative step were estimated from reaction rates and selectivities for pure C_3H_8 reactants. Fig. 8a shows experimental and predicted concentrations of C_3H_6 and C_1–C_2 products as a function of contact time. These parameters were then used to describe the results obtained during O_2 staging, for which CO_x formation rate constants (k_3) were estimated from CO_x formation rates. Data and model predictions are shown in Fig. 8b for 20 kPa C_3H_8 and the staging protocol in Table 1a. C_3H_6 yields during O_2 staging were accurately described at short contact times (< 2 ks), but the kinetic model predicted higher C_3H_6 yields than experimentally observed as contact time and C_3H_8 conversion increased. Measured C_3H_6 yields reached limiting values as conversion increases, while the model, which rigorously accounts for all thermodynamic effects, predicts a monotonic increase in C_3H_6 yields. This apparent decrease in forward C_3H_8 dehydrogenation rates with increasing contact time reflects a loss of catalytic sites, which does not occur with pure C_3H_8 reactants in batch reactors (Fig. 8a) or in long-term flow experiments (Fig. 2). Therefore, O_2, its reaction products H_2O and CO, or the concomitant high alkene/H_2 ratios prevalent for reactions of C_3H_8–O_2 mixtures led to deactivation or to kinetic inhibition of active sites during C_3H_8 dehydrogenation on Pt/Na-[Fe]ZSM5.

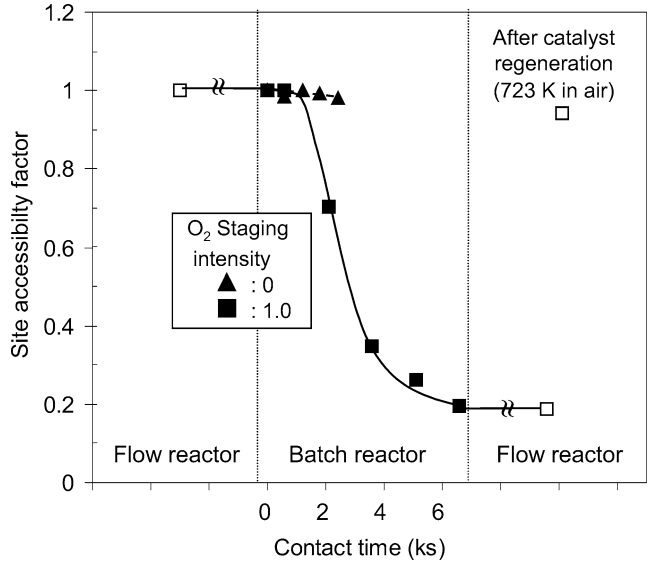

Fig. 9. Site accessibility factors for forward C_3H_6 formation rate on 0.1 wt% Pt/Na-[Fe]ZSM5 [flow reactor: 723 K, 18.6 mol C_3H_8/(g-atom Pt s), 20 kPa C_3H_8, balance He; batch reactor: 723 K, 20 kPa C_3H_8, O_2 staging protocol: (1) 0–0.3 ks without O_2, (2) 0.3–2.4 ks 0.23 mol/(g-atom Pt s), (3) 2.4–6.6 ks 0.14 mol/(g-atom Pt s), balance He; catalyst regeneration: 723 K, dry air, 2 h].

The extent of this deactivation or kinetic inhibition was described using a site accessibility factor (Φ), defined as the ratio of the experimental forward rate to that predicted by the kinetic model at each contact time. Values of Φ are shown in Fig. 9 for C_3H_8 reactions at 723 K and an O_2 staging efficiency of unity; they decrease from their initial value of

unity to ∼ 0.20 at 6.6 ks during experiments, but remain near unity at all contact times for pure C_3H_8 reactants.

Rate measurements in a flow reactor (723 K; 18.6 mol C_3H_8/(g-atom Pt s) space velocity) before and after semibatch O_2 staging experiments gave similar values of Φ (Fig. 9). These similar values indicate that loss of activity was not caused by kinetic inhibition of C_3H_8 dehydrogenation rates by H_2O or CO_x combustion products, but by irreversible titration of active sites. Treatment in dry air at 723 K for 2 h restored initial C_3H_8 dehydrogenation rates, suggesting that site blockage was caused by carbon deposition via CO disproportionation or alkene oligomerization and aromatization reactions. These reactions are favored as catalysts are exposed to high alkene and CO concentrations without the concurrent presence of H_2. The recovery of catalytic rates by oxidative treatments indicates that neither Pt sintering nor loss of zeolite crystallinity are responsible for the observed deactivation.

The effect of CO on deactivation rates was also probed by adding CO (0.025 kPa) to C_3H_8 reactants (20 kPa; 18.6 mol C_3H_8/(g-atom Pt s) space velocity) in a flow reactor at 793 K. Deactivation rate constants increased from 0.008 h^{-1} with pure C_3H_8 reactants to 0.06 h^{-1} when CO was added, suggesting that CO disproportionation reactions are involved in deactivation processes observed during cofeed experiments and, to a lesser extent, during O_2 staging. These experiments, however, overestimate the effects of CO in staged O_2 experiments because the catalyst bed is exposed to the entering reactant stream before any H_2 can be formed in dehydrogenation reactions. Also, staged O_2 addition led to higher C_{6+} selectivity (0.19% vs 0.075%; at ∼ 17% C_3H_8 conversion), suggesting that lower H_2 concentrations prevalent during O_2 staging favored oligomerization and aromatization reactions, which can also lead to unreactive unsaturated deposits.

Thus, precise control of O_2 introduction rates and local H_2 concentrations is required in order to overcome thermodynamic barriers in alkane dehydrogenation reactions, because of the need to avoid site blocking favored by high alkene/H_2 ratios and CO concentrations prevalent during O_2 staging. Optimum performance typically requires overall O_2 staging intensities slightly below stoichiometric values and O_2 introduction rates that vary with reactor position in tubular flow reactors or with contact time in semibatch reactors.

3.6. Comparison of O_2 staging with catalytic H_2 combustion

A previous study reported C_3H_8 dehydrogenation reactions coupled with H_2 combustion in a three-stage process designed to increase C_3H_6 yields above equilibrium values [25]. In this scheme, the first and third stages contained 0.7 wt% Pt–Sn[AL]ZSM5 (2 g) and the intermediate stage contained 10 wt% In_2O_3/ZrO_2 (0.1 g), which provided lattice oxygen atoms for selective combustion of H_2 formed in the first stage. Air was introduced into the middle stage in order to replenish lattice oxygen atoms as they reacted with H_2 to form H_2O. C_3H_8 rates and selectivities were compared with those achieved when the middle stage was bypassed (Table 5). The three-stage process gave 30% C_3H_6 yields with 99% C_3H_6 selectivity for an O_2/C_3H_8 ratio of 0.06. Higher O_2/C_3H_8 ratios (0.12) gave slightly higher C_3H_6 yields (33%), but lower selectivities (96%). These two O_2/C_3H_8 ratios gave C_3H_6 yields about 1.2–1.3 greater than the equilibrium values attainable without H_2 removal. These yield enhancements (1.2–1.3) are lower than those reported here at significantly lower temperatures using staged O_2 introduction (1.58) and a single-stage Pt/Na-[Fe]ZSM5 catalyst. Both this three-stage cyclic process [25] and our single-stage system gave low CO_x selectivities (< 5%) and high O_2 reactant efficiencies. Staging strategies, however, avoid the cyclic operation required in multistage systems, while using a single catalysts for selective combustion of H_2 and dehydrogenation of alkanes; these features markedly decrease process complexity and costs. Staged O_2 introduction can be implemented using multiple injectors in large-scale packed-bed or fluid-bed reactors. It can also be achieved using ceramic membranes as reactor walls, which can additionally separate pure O_2 from ambient air.

4. Conclusions

High C_3H_8 dehydrogenation rates with high alkene selectivities and yields and unprecedented catalyst stability were achieved using Pt clusters residing within shape-selective channels in Na-[Fe]ZSM5. These materials provide anchoring sites for Pt exchange, which lead to well-dispersed clusters during subsequent reduction, and much weaker acid sites than [Al]ZSM5 materials. Deactivation rate constants (∼ 0.008 h^{-1}) were much lower than on previously reported dehydrogenation catalysts and initial reaction rates and selectivity were recovered using mild oxidative treatments after 160 h on stream. Staged O_2 introduction led to the combustion of H_2 with ∼ 90% selectivity on these catalysts, even when hydrocarbons were predominant components in reacting mixtures. Alkene yields higher than equilibrium by a factor of ∼ 1.6 were achieved for C_2H_6 and C_3H_8 dehydrogenation at 773 and 723 K, respectively. These enhancement factors are significantly higher than previously reported with a more complex three-stage selective H_2 combustion scheme. Cofeeding alkane–O_2 reactant mixtures led to the rapid combustion of hydrocarbons and to the depletion of O_2 before H_2 is formed and dehydrogenation reactions approach equilibrium. High O_2 concentrations lead to CO formation and to H_2 depletion, both of which favor the formation of deactivating deposits. Thus, precise control of O_2 introduction location and rate is required in order to ensure that O_2 reactants become available as H_2 is formed in dehydrogenation reactions.

Acknowledgments

The authors acknowledge Darren P. Fong (ChevronTexaco Corp.) for technical assistance with the catalyst synthesis. One of the authors (T.W.) acknowledges the financial support of the Japan Cooperation Center, Petroleum and Nippon Oil Corporation, for his research activities at the University of California at Berkeley.

References

[1] M.M. Bhasin, J.H. McCain, B.V. Vora, T. Imai, P.R. Pujado, Appl. Catal. 221 (2001) 397.
[2] P.R. Pujado, B.V. Vora, Hydrocarbon Process. 69 (1990) 2140.
[3] R.O. Dunn, F.M. Brickmeyer, G.F. Schuette, in: Proceedings of the NPRA Annual Meeting, New Orleans, LA, 22–24 March, 1992.
[4] S. Gussow, R. Whitehead, in: Proceedings of the NPRA Annual Meeting, San Antonio, TX, 17–19 March, 1991.
[5] M. Boelt, H. Zimmermann, in: AIChE Spring Meeting, Houston, 1991.
[6] D. Sanfilippo, F. Buonomo, G. Fusco, M. Lupieri, I. Miracca, Chem. Eng. Sci. 47 (1992) 2313.
[7] O.A. Barias, A. Holmen, E.A. Blekkan, J. Catal. 158 (1996) 1.
[8] S.M. Stagg, C.A. Querini, W.E. Alvarez, D.E. Resasco, J. Catal. 168 (1997) 75.
[9] G. Meitzner, G.H. Via, F.W. Lytle, S.C. Fung, J.H. Sinfelt, J. Phys. Chem. 92 (1988) 2925.
[10] R.D. Cortright, J.A. Dumesic, Appl. Catal. 129 (1995) 101.
[11] J. Salmones, J.A. Wang, J.A. Galicia, G. Aguilar-Rios, J. Mol. Catal. 184 (2002) 203.
[12] Y.X. Li, K.J. Klabunde, B.H. Davis, J. Catal. 128 (1991) 1.
[13] F.M. Dautzenberg, J.N. Helle, P. Biloen, W.M.H. Sachtler, J. Catal. 63 (1980) 119.
[14] R.D. Cortright, J.A. Dumesic, J. Catal. 157 (1995) 576.
[15] H.H. Kung, Adv. Catal. 40 (1994) 1.
[16] E.A. Mamedov, V. Cortés Corberán, Appl. Catal. A 127 (1995) 1.
[17] S. Albonetti, F. Cavani, F. Trifirò, Catal. Rev.-Sci. Eng. 38 (1996) 413.
[18] T. Blasco, J.M. López Nieto, Appl. Catal. A 157 (1997) 117.
[19] M.A. Bañares, Catal. Today 51 (1999) 319.
[20] A. Khodakov, J. Yang, S. Su, A.T. Bell, E. Iglesia, J. Catal. 177 (1998) 343;
A. Khodakov, B. Olthof, A.T. Bell, E. Iglesia, J. Catal. 181 (1999) 205.
[21] A. Baretta, P. Forzatti, E. Ranzi, J. Catal. 184 (1999) 469.
[22] J. Collins, R. Schwarz, R. Sehgal, T. Ward, C. Brinker, G. Hagen, C. Udovich, Ind. Eng. Chem. Res. 35 (1996) 4398.
[23] C.M. Reo, L.A. Bernstein, C.R.F. Lund, Chem. Eng. Sci. 52 (1997) 3075.
[24] T. Imai and D.Y. Jan, US patent 4,788,371, 1998.
[25] R.K. Grasselli, D.L. Stern, J.G. Tsikoyiannis, Appl. Catal. 189 (1999) 1;
R.K. Grasselli, D.L. Stern, J.G. Tsikoyiannis, Appl. Catal. 189 (1999) 9.
[26] T. Waku, J.A. Biscardi, E. Iglesia, Chem. Commun. 1764 (2003).
[27] J. Houzvicka, J.G. Nienhuis, S. Hansildaar, V. Ponec, Appl. Catal. A 165 (1997) 443.
[28] E. Iglesia, J.E. Baumgartner, G.L. Price, K.D. Rose, J.L. Robbins, J. Catal. 125 (1990) 95.
[29] L.A. Bernstein, C.M. Reo, C.R.F. Lund, J. Membr. Sci. 118 (1996) 93.
[30] H.S. Fogler, Elements of Chemical Reaction Engineering, Prentice Hall, New Jersey, 1999.
[31] D.R. Stull, E.F. Westrum Jr., G.C. Sinke, The Chemical Thermodynamics of Organic Compounds, Willey, New York, 1969.
[32] D. Kahaner, C. Moler, S. Nash, Numerical Methods and Software, Prentice Hall, 1988.
[33] J.H. Sinfelt, Catal. Lett. 9 (1991) 159.
[34] J.A. Biscardi, E. Iglesia, J. Phys. Chem. B 102 (1998) 9284.
[35] J.A. Biscardi, E. Iglesia, J. Catal. 182 (1999) 117.
[36] O. Kresnawahjuesa, G.H. Kuhl, R.J. Gorte, C.A. Quierini, J. Catal. 210 (2002) 106.
[37] L. Bednarova, C.E. Lyman, E. Rytter, A. Holmen, J. Catal. 211 (2002) 355.
[38] Y. Zhou, S.M. Davis, US patent 5,214,227, 1993.
[39] S.A.I. Barri, US patent 4,665,267, 1987.
[40] S.A.I. Barri, R. Tahir, US patent 5,126,502, 1992.
[41] T. Waku, S.Y. Yu, E. Iglesia, Ind. Eng. Chem. Res. 3680 (2003) 42.
[42] C.J. Sun, C.J. Sung, L. He, C.K. Law, Combust. Flame 118 (1999) 108.
[43] A.H. McDaniel, A.E. Lutz, M.D. Allendorf, S.F. Rice, J. Catal. 208 (2002) 21.